Journal of Biomolecular NMR **29:** 351–361, 2004.

Site-specific labelling with a metal chelator for protein-structure refinement

Guido Pintacuda[a], Ahmad Moshref[a], Ainars Leonchiks[b], Anatoly Sharipo[b] & Gottfried Otting[c,*]

[a]*Department of Medical Biochemistry and Biophysics, Karolinska Institute, S-171 77 Stockholm, Sweden;* [b]*Biomedical Research and Study Centre, University of Latvia, LV-1067 Riga, Latvia;* [c]*Research School of Chemistry, Australian National University, Canberra, ACT 0200, Australia*

Received 24 December 2003; Accepted 3 March 2004

Key words: inversion-recovery, paramagnetic relaxation enhancement, paramagnetic restraints, protein derivatization, S-cysteaminyl-EDTA

Abstract

A single free Cys sidechain in the N-terminal domain of the *E. coli* arginine repressor was covalently derivatized with S-cysteaminyl-EDTA for site-specific attachment of paramagnetic metal ions. The effects of chelated metal ions were monitored with ^{15}N-HSQC spectra. Complexation of Co^{2+}, which has a fast relaxing electron spin, resulted in significant pseudocontact shifts, but also in peak doubling which was attributed to the possibility of forming two different stereoisomers of the EDTA-Co^{2+} complex. In contrast, complexation of Cu^{2+} or Mn^{2+}, which have slowly relaxing electron spins, did not produce chemical shift changes and yielded self-consistent sets of paramagnetic relaxation enhancements of the amide protons. T_1 relaxation enhancements with Cu^{2+} combined with T_2 relaxation enhancements with Mn^{2+} are shown to provide accurate distance restraints ranging from 9 to 25 Å. These long-range distance restraints can be used for structural studies inaccessible to NOEs. As an example, the structure of a solvent-exposed loop in the N-terminal domain of the *E. coli* arginine repressor was refined by paramagnetic restraints. Electronic correlation times of Cu^{2+} and Mn^{2+} were determined from a comparison of T_1 and T_2 relaxation enhancements.

Introduction

Introduction of a paramagnetic centre into an otherwise diamagnetic macromolecule (spin-labelling) provides a rich source of additional structural information, since paramagnetic restraints extend over much larger distances than NOEs. Straightforward parameters are relaxation enhancements and pseudo-contact shifts observed for the nuclear spins of the macromolecule (Bertini and Luchinat, 1996). In addition, anisotropic magnetic susceptibility of the paramagnetic centre causes an alignment of the molecule with respect to the external magnetic field, enabling the measurement of residual dipolar couplings (Tolman et al., 1995; Prosser et al., 1999; Ma and Opella, 2000; Barbieri et al., 2002a,b). Recently, cross-correlated relaxation with the Curie spin of the paramagnetic centre has been shown to provide long-range angular information (Boisbouvier et al., 1999; Madhu et al., 2002; Pintacuda et al., 2003). Restraints from paramagnetic data are readily included in protein structure determinations (Bertini et al., 1996, 1997, 2000; Banci, 1998; Hus et al., 2000; Barbieri et al., 2002a; Bertini, 2002). In a reverse application, paramagnetic data can also be used to obtain resonance assignments for proteins of known three-dimensional structure (Pintacuda et al., 2004).

The most frequently used spin labels are nitroxide compounds. Reagents which attach the nitroxide spin label via a disulphide bond to cysteine residues are commercially available and have been used ex-

*To whom correspondence should be addressed. E-mail: go@rsc.anu.edu.au

tensively to derive structural information by NMR (Hubbell and Altenbach, 1994; Hubbell et al., 1998; Girvin and Fillingame, 1995; Papavoine et al., 1995; Gillespie and Shortle, 1997a,b; Ramos and Varani, 1998; Johnson et al., 1999; Battiste and Wagner, 2000; Gaponenko et al., 2000, 2004; Varani et al., 2000; Liu et al., 2002). Nitroxide labels are characterized by an isotropic magnetic susceptibility, resulting in slowly relaxing electron spins and strong relaxation enhancements, but no pseudocontact shift information.

A more attractive approach is presented by the site-directed attachment of a metal chelator, as this allows the binding of metal ions with different paramagnetic properties. Reagents for connecting a metal chelator to amino-acid side chains have been developed for radiolabeling of monoclonal antibodies (Liu and Edwards, 2001), fluorescent studies (Selvin, 2002) and metal-promoted oxidative cleavage reactions (Ebright et al., 1992, 1993). These reagents, however, usually do not achieve site-specific labelling. In addition, they often contain a long linker, resulting in ill-defined positioning of the metal ion with respect to the protein. Consequently, different metal-binding peptide motifs have been proposed for N- or C-terminal fusion to proteins: a zinc-finger tag (Gaponenko et al., 2000a), a three-residue peptide flanked by two His residues, His-X_3-His (Voss et al., 1995), an EF-hand calcium-binding site (Ma and Opella, 2000) or three-residue Cu^{2+}-binding sequences (Donaldson et al., 2001; Mal et al., 2002). Calcium-binding sites are of particular interest, as they have the potential to bind lanthanides, allowing the measurement of paramagnetic effects in different distance ranges (Allegrozzi et al., 2000). Improved N-terminal peptide sequences are available which have been optimized for lanthanide binding (Wöhnert et al., 2003). Recently, however, S-(2-pyridylthio)-cysteaminyl-EDTA (Scheme 1) became commercially available (TRC, Toronto, Canada). This reagent allows the specific and quantitative derivatization of cysteine thiol groups with an S-cysteaminyl-EDTA moiety and has been shown to generate highly useful NMR restraints when complexed with different paramagnetic metal ions, including lanthanides (Dvoretsky et al., 2002; Gaponenko et al., 2002, 2004). In particular, significant pseudocontact shifts and residual dipolar couplings could be measured for metal ions with rapidly relaxing electron spins (Dvoretsky et al., 2002).

In the present work, the generality of the use of S-(2-pyridylthio)-cysteaminyl-EDTA was investigated by studying the 78-residue, ^{15}N-labelled N-terminal domain of the *E. coli* arginine repressor (ArgN; Sunnerhagen et al., 1997), derivatized at the single cysteine residue present in the wild-type protein. The results indicate that this reagent works well for measuring paramagnetic relaxation enhancements caused by metal ions with slowly relaxing electron spins, while metal ions with rapidly relaxing electron spins result in peak doubling and spectra that can be difficult to interpret. A protocol was established for identification of the metal position from paramagnetic relaxation enhancement data which allowed refinement of the structure of a solvent-exposed loop with low NOE density.

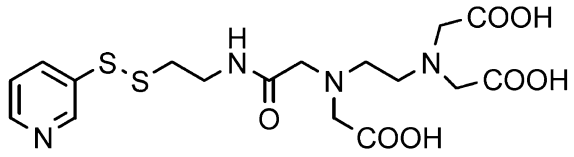

Scheme 1.

Experimental section

Sample preparation

^{15}N-labelled ArgN was expressed and purified as described (Sunnerhagen et al., 1997). Site-specific labelling of Cys68 of ArgN was achieved by a procedure similar to that described by Gaponenko et al. (2002). 10 ml of a 50 μM protein solution were pretreated for 3 h with about 3 mM DTT to reduce all free cysteine thiol groups. Subsequently, the buffer was exchanged using an Amicon concentrator (Millipore, 5000 MW cutoff) for 50 mM Tris buffer (pH 8.0) containing 100 mM NaCl and 1 mM EDTA. A ten-fold excess of S-(2-pyridylthio)-cysteaminyl-EDTA (Toronto Research Chemicals) was added and the mixture incubated at room temperature for 3 h. The reaction was monitored spectrophotometrically, using the absorption band of pyridylthione (ε_{343} = 8080 $cm^{-1}M^{-1}$) which is a product of the reaction. The reaction was virtually complete after 1 h. Mass spectrometric analysis indicated > 95% derivatization. Excess reagent and any side products were removed by exchanging the buffer for 20 mM 2-(N-morpholino)ethanesulfonic acid (MES; pH 6.5), 50 mM NaCl, 90% H_2O/10% D_2O, using an Amicon concentrator (Millipore, 5000 MW cutoff). 50 μM solutions of derivatized ArgN were used to coordinate different metal ions ($MnCl_2$, $CuCl_2$, $ZnCl_2$, $CoCl_2$

and $GdCl_3$). The metal salts were used in 10% excess and any uncoordinated metal ions removed by the addition of 10 µl of Chelex-100 beads (Aldrich). The supernatant of the beads was concentrated to final protein concentrations of between 0.3 to 1 mM. Several rounds of dilution with 700 mM NaCl and subsequent re-concentration by ultrafiltration were necessary in addition to eliminate metal binding at alternative sites of the protein.

NMR spectroscopy

All NMR experiments were recorded at 25 °C using a Bruker DMX-600 NMR spectrometer equipped with a cryoprobe. A 3D NOESY-^{15}N-HSQC spectrum (50 ms mixing time, $t_{1\max}$ = 60.0 ms, $t_{2\max}$ = 45.9 ms, $t_{3\max}$ = 91.7 ms, 4 scans per FID) was recorded on the diamagnetic EDTA-derivatized sample in order to verify the resonance assignments of the ^{15}N-HSQC cross peaks. $^1H^N-^{15}N$ residual dipolar couplings were measured by ^{15}N-HSQC-α,β experiments (Andersson et al., 1998) in diamagnetic and Co^{2+}-EDTA-derivatized ArgN. Possible exchange between different ^{15}N-HSQC cross peaks of the Co^{2+}-substituted sample was investigated with the [^{1}H,^{15}N]-two-spin-order exchange difference experiment (Wider et al., 1991), using mixing times of 40 and 400 ms.

Non-selective T_1 relaxation times of the amide H^N resonances were measured by ^{15}N-HSQC experiments preceded by a 180°(^{1}H) pulse and a relaxation delay (Farrow et al., 1994). Between seven and ten experiments with relaxation delays in the range between 5 ms and 2.2 s were recorded to measure the T_1 values of EDTA-derivatized ArgN, using an interscan recovery delay of 5 s. The measured peak intensities were fitted to a three-parameter exponential equation (Ferretti and Weiss, 1989).

Paramagnetic enhancements of the R_2 relaxation rates of the amide H^N resonances of Cu^{2+}- and Mn^{2+}-EDTA-derivatized ArgN and diamagnetic EDTA-derivatized ArgN were measured in two ways, (i) by evaluating the exponential decays of the cross-peak intensities in a spin-echo ^{15}N-HSQC experiment with a selective refocusing pulse applied to the amide protons as described by Donaldson et al. (2001), recorded with variable relaxation delays between 11 and 100 ms, and (ii) by comparison of the full line widths at half-height L^{p} and L^{d} in the ^{1}H dimension of ^{15}N-HSQC spectra of the paramagnetic and the diamagnetic protein, respectively, using the equation

$$R_2^{\mathrm{p}} = \pi(L^{\mathrm{p}} - L^{\mathrm{d}}) \tag{1}$$

and disregarding the presence of scalar couplings.

The rotational correlation time of ArgN was determined by measurements of the T_1 and T_2 relaxation times of the ^{15}N nuclei in a series of one-dimensional experiments recorded with ^{1}H detection (Farrow et al., 1994).

Paramagnetic relaxation enhancements

The paramagnetic contribution to the longitudinal (R_1^{p}) and transverse (R_2^{p}) relaxation rates were determined by subtracting the values measured for diamagnetic EDTA-derivatized ArgN from those measured for the paramagnetic samples. For slowly relaxing metal ions like Cu^{2+} and Mn^{2+}, the paramagnetic relaxation rate R_1^{p} and R_2^{p} follow the Solomon-Bloembergen equation (Banci et al., 1991) as:

$$R_1^{\mathrm{p}} = \frac{2}{15}\left(\frac{\mu_0}{4\pi}\right)^2 \frac{\gamma_{\mathrm{H}}^2 (g\mu_{\mathrm{B}})^2 S(S+1)}{r^6} \left(\frac{3\tau_{\mathrm{c}}}{1+\omega_{\mathrm{H}}^2\tau_{\mathrm{c}}^2} + \frac{7\tau_{\mathrm{c}}}{1+\omega_{\mathrm{S}}^2\tau_{\mathrm{c}}^2}\right) = \frac{K_1}{r^6}, \tag{2}$$

$$R_2^{\mathrm{p}} = \frac{1}{15}\left(\frac{\mu_0}{4\pi}\right)^2 \frac{\gamma_{\mathrm{H}}^2 (g\mu_{\mathrm{B}})^2 S(S+1)}{r^6} \left(4\tau_{\mathrm{c}} + \frac{3\tau_{\mathrm{c}}}{1+\omega_{\mathrm{H}}^2\tau_{\mathrm{c}}^2} + \frac{13\tau_{\mathrm{c}}}{1+\omega_{\mathrm{S}}^2\tau_{\mathrm{c}}^2}\right) = \frac{K_2}{r^6}, \tag{3}$$

where μ_0 is the vacuum permeability, γ_{H} the proton gyromagnetic ratio, μ_{B} the Bohr magneton, r the proton-metal distance, ω_{H} and ω_{S} the Larmor frequencies of the proton and electron spin, respectively, and the effective correlation time τ_{c} depends on the molecular rotational correlation time τ_{r} and the electronic relaxation time τ_{e} as

$$1/\tau_{\mathrm{c}} = 1/\tau_{\mathrm{r}} + 1/\tau_{\mathrm{e}}. \tag{4}$$

In the absence of EPR data on the specific complexes investigated here, the ion g factor was assumed to be 2.00 for both Cu^{2+} and Mn^{2+} (Banci et al., 1991).

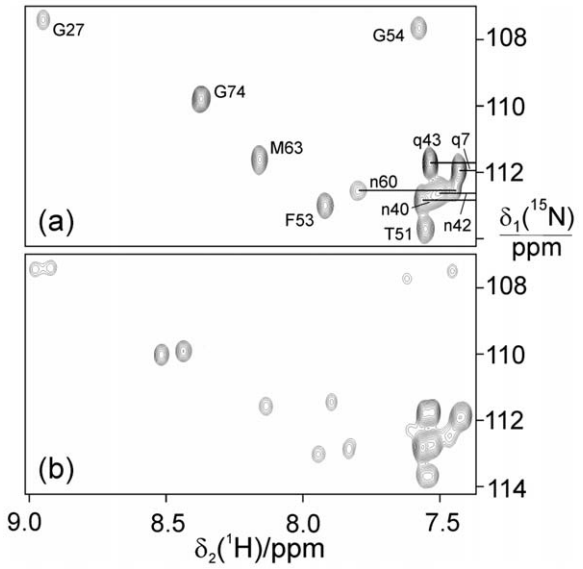

Figure 1. ^{15}N-HSQC spectra of a ca. 1 mM solution of EDTA-derivatized ArgN in 90% H_2O/10% D_2O at pH 6.5 and 25 °C. (a) No paramagnetic ion present. Cross-peaks are labeled by their amino acid type and residue number. Small characters identify cross-peaks from side-chain amides. (b) 1:1 complex with Co^{2+}.

Structure calculations

NMR structure calculations were performed using the program DYANA (Güntert et al., 1997), starting from 50 random conformers. The published coordinates of ArgN (pdb code 1AOY, Sunnerhagen et al., 1997) were used to create a set of 1704 upper-distance restraints that reflect the conformational spread between the 23 NMR conformers. Restraints were created only for ^{1}H-^{1}H distances which are shorter than 4.5 Å in all NMR conformers, each restraint corresponding to the longest distance found for the respective ^{1}H-^{1}H pair in any of the NMR conformers. Structures calculated with these restraints closely reproduced the rmsd values of the original NMR structure. In particular, the average rmsd value for the heavy atoms of residues 57 to 65 of the structure calculated with these restraints was within 3% of that of the original structure.

A preliminary position of the metal ion was determined by minimizing the expression

$$T = \sum_i \left(R^{\mathrm{p}}_{1,i} - \frac{K_1}{r_i^6} \right)^2 . \qquad (5)$$

The sum runs over all amide protons of the lowest-energy NMR structure. The minimization led to simultaneous optimization of the metal ion coordinates and of the factor K_1 which depends on the total correlation time τ_c. Minimizations starting from τ_c values in the range of 1 to 20 ns and metal positions varying about the position of the cysteine SH by ±10 Å resulted in the same metal position and correlation time. The conversion of experimental R_1^{p} values to distance restraints was subsequently achieved as proposed by Bertini et al. (1996). In this procedure, $(R_1^{\mathrm{p}})^{1/6}$ was plotted versus the distances r_i between the protons i and the metal position determined by the initial fit. The straight lines lying just above and below the points in the plot were taken as the calibration curves for upper and lower distance limits, respectively. In the subsequent DYANA calculations, the metal ion was described by a pseudo-residue connected to the C-terminus of the protein by a mass-free 10-residue linker. Calculations were performed with and without paramagnetic distance restraints.

Results

Diamagnetic EDTA-derivatized ArgN

Derivatization of ArgN with S-cysteaminyl-EDTA resulted in few changes in ^{1}H chemical shifts that were confined to the local environment of Cys68 and smaller than 0.15 ppm. Complexation with Zn^{2+} did not result in further chemical shift changes which might be expected, if EDTA were complexed with Na^+ in the absence of divalent metal cations. T_1 values measured in the presence and absence of Zn^{2+} were indistinguishable. A 3D NOESY-^{15}N-HSQC spectrum was used to verify the resonance assignments of the ^{15}N-HSQC spectrum. ^{15}N-HSQC cross-peaks could be identified for 68 of the 72 non-proline residues. The missing signals were from the amino-terminal residues which exchanged rapidly with the water.

Co^{2+} complex

Figure 1 shows the effect of Co^{2+} on the ^{15}N-HSQC spectrum of EDTA-derivatised ArgN. Compared to the ^{15}N-HSQC spectrum of diamagnetic EDTA-derivatized ArgN (Figure 1a), the peaks are doubled into two sets of similar intensity in the presence of the metal ion (Figure 1b). This effect is readily explained by the presence of two diastereomers of the EDTA-Co^{2+} complex, as proposed by Griesinger and co-workers (Ikegami et al., 2004). Although locally confined, the effect of the conformational heterogeneity is visible over the entire molecule since the anisotropic magnetic susceptibility tensors have different

orientations for the two diastereomers. No chemical exchange between the two forms could be detected with mixing times of 400 ms. Consequently, resonance assignments for the different stereoisomers were difficult to obtain for this complex, although the chemical shift changes were smaller than about 0.3 ppm. The absence of cross-peaks from diamagnetic ArgN illustrated the high yield of the derivatization reaction. Residual dipolar couplings between −3 and 3 Hz were measured for those amide cross-peaks which could be resolved and assigned for both species. Different values measured for the same residues in both species indicated different orientational alignments for the two stereoisomers.

Cu^{2+} and Mn^{2+} complexes

The absence of low-lying excited states for Cu^{2+}, Mn^{2+} and Gd^{3+} results in slowly relaxing electronic spins ($\tau_e > 10^{-9}$s). In addition, the magnetic susceptibility is isotropic or, as in the case of Cu^{2+}, close to isotropic, so that these metal ions generate no or negligable pseudocontact shifts or molecular alignments in a magnetic field, but cause strong relaxation rate enhancements for proton spins with a simple distance dependence from the metal ion (equations 2 and 3). The relaxation enhancements are thus insensitive with regard to subtle differences in metal ion coordination.

Figure 2 shows the effect of complexation with Cu^{2+} and Mn^{2+}, respectively, on the ^{15}N-HSQC spectrum of EDTA-derivatized ArgN. As expected, no changes in chemical shifts or peak doublings are observed. Only a few cross-peaks are strongly broadened in the case of Cu^{2+}, while almost all resonances broaden in the case of Mn^{2+}, where the relaxation enhancement is amplified by the larger electronic spin and slower electronic relaxation. In both cases, some of the amide cross-peaks were broadened beyond detection, resulting in 64 and 38 observable cross-peaks (out of 68) in the presence of Cu^{2+} and Mn^{2+}, respectively.

In the case of the Cu^{2+} complex, intermolecular relaxation did not seem to interfere with the measurements, as the measured rates were independent of protein concentration in the range between 0.2 and 1 mM.

In the case of the Mn^{2+} complex, significant R_2^p values were measured for the amide protons of residues 43 and 44 and of the side chains of residues Gln 28 and Gln 43 although these residues are located far from the EDTA moiety. This effect was attenuated at lower protein concentrations, indicating that it was due to intermolecular relaxation enhancement. As noted earlier, ArgN possesses a pronounced electric dipole moment (Sunnerhagen et al., 1997). Possibly, the negatively charged EDTA moiety is attracted to the positive charge potential around residues 43 and 44. Consequently, the relaxation data of these two residues were omitted from the analysis presented in Figure 4.

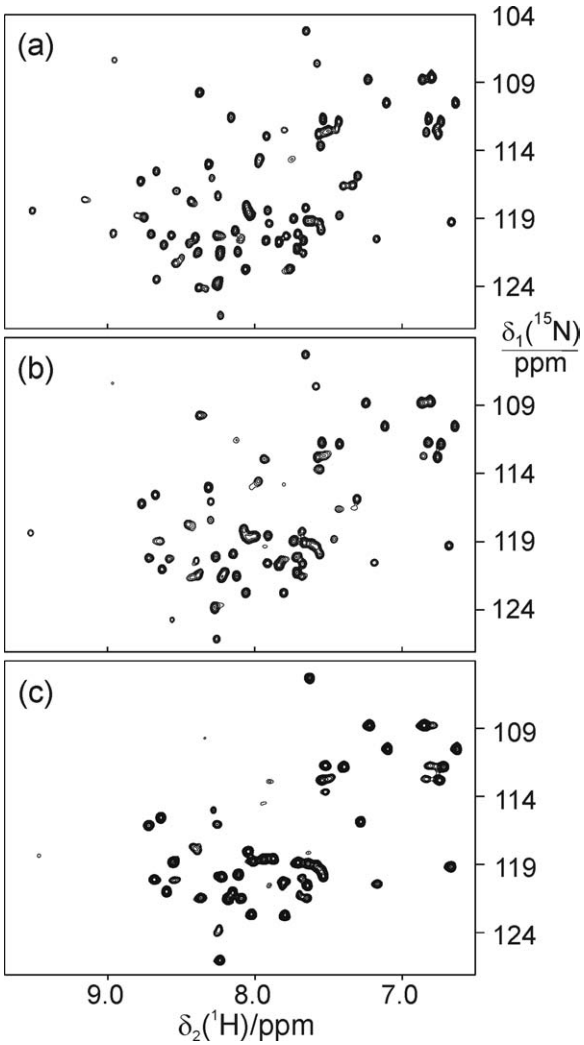

Figure 2. ^{15}N-HSQC spectra of a ca. 1 mM solution of EDTA-derivatized ArgN in 90% H_2O/10% D_2O at pH 6.5 and 25 °C. (a) No paramagnetic ion present. (b) 1:1 complex with Cu^{2+}. (c) 1:1 complex with Mn^{2+}.

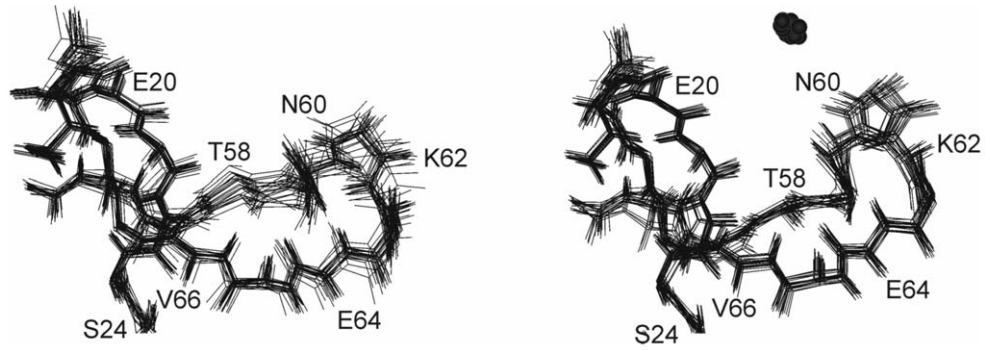

Figure 3. Families of twenty ArgN conformers calculated (a) with 1704 NOE-distance restraints and (b) with the inclusion of 60 additional paramagnetic relaxation restraints from the Cu^{2+} complex. Overlapping spheres mark the position of the Cu^{2+} ion in the different conformers. Only the backbone heavy atoms are displayed for residues 19–25 and 55–68.

Structure calculation with paramagnetic distance restraints

The paramagnetic contributions R_1^p and R_2^p to the longitudinal and transverse relaxation rates of the amide protons could be measured quantitatively for sixty well-resolved signals of Cu^{2+}-EDTA-derivatized ArgN. Although the presence of two diastereomers must be assumed as in the case of the Co^{2+} complex, the cross-peak intensities could be fitted with single exponentials. There was no evidence that the position of the metal varied significantly between the two diastereomers.

The R_1^p values measured for Cu^{2+}-EDTA-derivatized ArgN were translated into distance restraints (see Materials and methods). About one third of the sixty measured R_1^p values resulted in meaningful distance restraints. The restraints were used together with NOE restraints in structure calculations with the program DYANA (Güntert et al., 1997), simultaneously yielding the metal position with respect to the protein and increased precision of the protein structure. The resulting structures did not violate any of the paramagnetic distance restraints. The structural definition was enhanced primarily near the metal ion (Figure 3), while the overall rmsd values varied only little (0.42 Å for the backbone atoms of residues 7–71, compared to 0.45 Å without paramagnetic restraints). The improvement in structural definition was particularly noticeable for the solvent exposed loop region comprising residues 58 to 65 for which conventional long-range distance restraints were scarce (Figure 3).

Superimposing the backbone atoms of the ArgN conformers, the position of the copper ion is determined with an rmsd of 0.4 Å. The position correctly predicts the disappearance of the signals that were broadened beyond detection in the ^{15}N-HSQC spectrum. The amide protons of these cross-peaks are all closer than 9 Å to the copper ion. Although the S-cysteaminyl-EDTA moiety was not explicitly modelled in the calculation, an extended conformation of the cysteaminyl chain would be able to bridge the coordinates of the sulfur atom of Cys68 and the metal atom and could be accommodated in the determined set of structures without any steric clashes with backbone or side chain atoms.

The measured paramagnetic relaxation enhancements displayed the expected $1/r^6$ dependence (Figure 4a). Experimental and back-calculated rates correlated more closely for R_1^p than R_2^p rates (Figure 4, d and e). In both cases, a τ_c value of 1.0 ± 0.1 ns was derived from K_1 and K_2 (Equations 2 and 3), respectively. Combined with a rotational correlation time of $\tau_r = 4.8 \pm 0.3$ ns, which was determined from ^{15}N relaxation measurements, this result indicated an electronic relaxation time τ_e of 1.3 ± 0.2 ns (Figure 4c).

Although the absolute error in the relaxation measurements increased with increasing relaxation rate enhancements (Figure 4a), shorter distances from the metal ion were measured with greater accuracy than longer distances, where the paramagnetic relaxation enhancement contributed relatively little to the total relaxation (Figure 4f). Distance measurements by R_1^p data were thus most accurate in the range between about 9 and 18 Å, while transverse relaxation rates were beset with a larger uncertainty for distances beyond about 15 Å (Figure 4f).

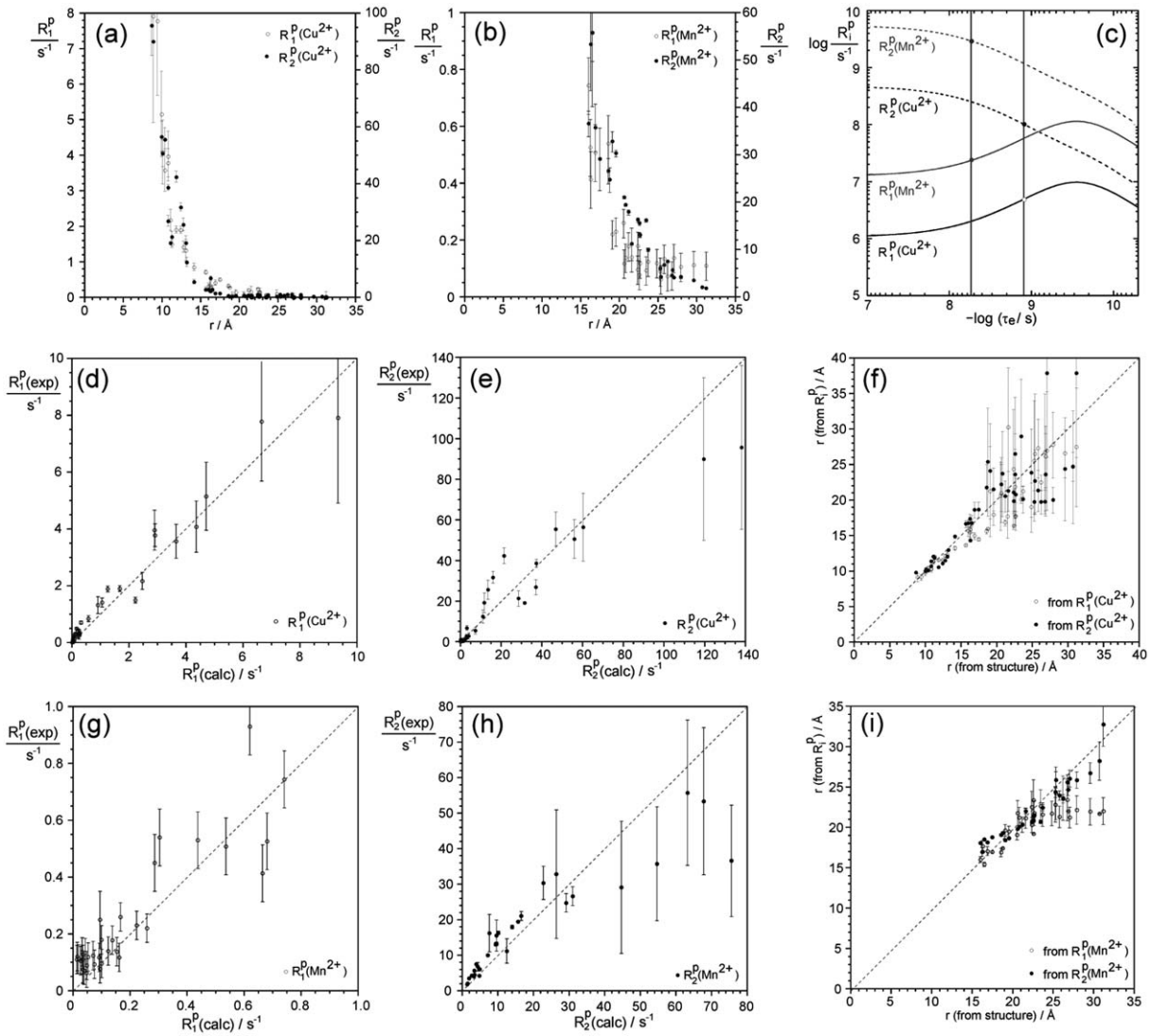

Figure 4. Paramagnetic relaxation rate enhancements of amide protons in EDTA-derivatized ArgN and correlations with back-calculated values and proton-metal distances in complexes with Cu^{2+} and Mn^{2+}. Data from residues 5–9 and 70–78 were omitted, since these regions were highly disordered in the NMR structure due to increased mobility. (a, b) Enhancement of the longitudinal and transverse relaxation rates of the amide protons of ArgN due to paramagnetic relaxation enhancements R_1^{p} (open circles) and R_2^{p} (filled circles) as a function of the proton-to-metal distance r in (a) the Cu^{2+} and (b) Mn^{2+} complexes. R_1^{p} (R_2^{p}) values were determined as the difference between the R_1 (R_2) relaxation rates measured for the paramagnetic metal-protein complexes and the diamagnetic protein. The distances were measured in the lowest-energy ArgN conformer of Figure 3. (c) Paramagnetic relaxation rate enhancements R_1^{p} (dashed lines) and R_2^{p} (continuous lines) *versus* the electronic correlation time τ_{e} in the case of a metal ion with electronic spin S = 1/2 (as in the case of Cu^{2+}) and S = 5/2 (as in the case of Mn^{2+}) and a rotational correlation time $\tau_{\mathrm{r}} = 4.8$ ns (as determined for ArgN). The values were calculated for a hypothetical proton at a distance of 1 Å from the metal; the vertical lines identify the electronic correlation times corresponding to the experimentally determined ratios of K_1 and K_2 (equations 2–4) for the Cu^{2+} and Mn^{2+} samples. (d and e) Correlation between experimental and back-calculated longitudinal and transverse paramagnetic relaxation rate enhancements for the Cu^{2+} complex. (f) Correlation between the metal-to-proton distances experimentally determined from relaxation data (R_1, open circles; R_2, filled circles) and the distances measured in the lowest-energy ArgN conformer for the Cu^{2+} complex. (g–i) Same as (d–f), except that the data pertain to the Mn^{2+} complex. R_1^{p} data for Cu^{2+} and R_2^{p} data for Mn^{2+} show the best linear behaviour in the ranges of 9–18 Å and 16–25 Å, respectively.

Distance restraints from Mn^{2+}

Due to the larger electronic moment of Mn^{2+}, the cross-peaks of amide protons closer than 16 Å to the metal were broadened beyond detection in the Mn^{2+}-EDTA-derivatized ArgN complex. Distance-dependent relaxation enhancements were measurable for distances in the relatively narrow range between 17 and 25 Å (Figure 4b). Compared to the corresponding complex with Cu^{2+}, this distance range is much longer, resulting in a very shallow minimum, when we attempted to determine the position of the metal ion with respect to the protein by the use of equation 5. The metal position determined for Cu^{2+}-EDTA-derivatized ArgN was, however, perfectly compatible with the R_1^p and R_2^p data measured for the Mn^{2+} complex. Back-calculated longitudinal and transverse relaxation rates based on this ion position correlated well with the experimental data (Figure 4, g and h), indicating a τ_c value of 2.5 ± 0.2 ns and, hence, a τ_e value of 5.4 ± 0.4 ns (Figure 4c).

In contrast to the situation of Cu^{2+}-driven relaxation, R_2^p data of the Mn^{2+}-complex proved to be more reliable than R_1^p data, in particular for longer distances from the metal ion (Figure 4i). Notably, non-vanishing R_1^p relaxation enhancements were still observed for very long distances from the metal (Figure 4b). This effect may be attributed to magnetization transfer between the water and the protein magnetization during the recovery delay of the inversion-recovery experiments which becomes noticeable during the long recovery delays needed to measure small relaxation enhancements. This magnetization transfer, which is effected by chemical exchange between water and amide protons and exchange-relayed NOEs, provides efficient coupling of the magnetizations of water and amide protons. As the Mn^{2+} ion enhances the relaxation rate of the water magnetization much more efficiently than Cu^{2+} (Banci et al., 1991), amide protons with strong coupling to the reservoir of water magnetization would be expected to relax with rates more similar to the relaxation rate of the water resonance. The biggest outlayers in Figure 4i were indeed from those amide protons for which the biggest cross-peaks with the water were observed in the 3D NOESY-^{15}N-HSQC spectrum of diamagnetic EDTA-derivatized ArgN (data not shown).

In the case of the Mn^{2+} complex, the pronounced line-broadening caused by the paramagnetic relaxation enhancement allowed the determination of reliable R_2^p values also from straightforward line-width measurements (data not shown). Although line-width measurements from a single spectrum are faster than the recording of a series of spectra for relaxation measurements, line-width measurements are compromised by cross-peak overlap. Therefore, only R_2^p values determined by relaxation measurements were included in Figure 4.

Gd^{3+} complex

As expected, the Gd^{3+} complex of ETDA-derivatized ArgN showed broad lines, with resonances of amide protons within 18 Å of the EDTA ligand broadened beyond detection (data not shown). Line broadenings were, however, observed for residues far from the EDTA attachment site in this complex, indicating the presence of more than a single binding site for the metal which could not be suppressed even by extensive washing with high concentrations of NaCl. This effect could be explained by intermolecular binding events, where natural metal binding sites on the protein surface complete the coordination sphere of EDTA-bound Gd^{3+}, since EDTA can only satisfy 6 of the 9 coordination sites of the lanthanide.

R_1^p versus R_2^p measurements

Figure 4c shows that the correlation between experimental and back-calculated paramagnetic relaxation enhancements is best for R_1^p data of the Cu^{2+} complex in the distance range up to about 9 to 18 Å, while R_2^p data of the Mn^{2+} complex data provided the best correlation at distances between 16 and 25 Å from the metal ion. Notably, the R_2^p rates measured for the Mn^{2+} complex were about 60 times faster than the R_1^p rates (Figure 4b), while the R_2^p rates measured for the Cu^{2+} complex were only about 12 times faster than the R_1^p rates (Figure 4a). The enhanced line-broadening of the Mn^{2+} complex, also evidenced in the ^{15}N-HSQC spectrum of Figure 1c, supported the accurate measurement of R_2^p rates, but resulted in poor sensitivity for R_1^p measurements by inversion recovery experiments. In contrast, R_1^p data measured for the Cu^{2+} complex were at least as accurate as R_2^p data. Different ratios between R_1^p and R_2^p relaxation rates for different metal ions are predicted by Equations 2 and 3 as a consequence of different electronic correlation times τ_e (Figure 4c). The experimentally determined factors K_1 and K_2 (Equations 2 and 3) thus provide access to this parameter which is difficult to measure otherwise, in particular as the electronic relaxation time of

Mn^{2+} strongly depends on the magnetic field strength (Koenig and Brown, 1985; Bertini et al., 1993). As expected, the electronic correlation time derived in this way was longer for the Mn^{2+} ion than for the Cu^{2+} ion (Figure 4c), reflecting the complete absence of intraconfigurational excited states for the former ion.

Discussion

Site-specific attachment of a metal complexation agent to proteins provides a promising tool for improving protein structure determinations by the recruitment of paramagnetic long-range restraints. The particular reagent used here, S-(2-pyridylthio)-cysteaminyl-EDTA, has the advantage of commercial availability, capability of cysteine derivatization with near-quantitative yields, and possibility of monitoring the progress of the derivatization reaction spectroscopically. A previous study using this reagent did not report problems of peak doubling with metal ions which generate pseudocontact shifts (Dvoretsky et al., 2002). This feature could be explained, if the protein environment favours one diastereomer of the EDTA-metal complex over the other. In our hands, peak doubling was observed with Co^{2+}.

In the present study, we restricted the quantitative analysis to metal ions with slow electronic relaxation, such as Cu^{2+} and Mn^{2+}. These ions do not change chemical shifts, obliterating the need of reassigning the cross-peaks in the ^{15}N-HSQC spectrum. The strong enhancements of ^{1}H relaxation confered by these metals have a simple distance dependence, providing valuable long-range distance information which is insensitive with respect to the existence of two different diastereomers of the EDTA-metal complex. The dissociation constants of the EDTA complexes of either metal ion are smaller than 10^{-13} M (Martell et al., 1972).

In principle, the measurement of R_1^p and R_2^p values can be affected by a number of systematic errors. For example, determination of R_2^p values by simple line-width measurements according to Equation 1 neglects the presence of $J(H^N,H^\alpha)$ coupling constants and will be acceptably accurate only for large R_2^p values. Similarly, measurement of small R_1^p values by non-selective inversion-recovery experiments is complicated by non-exponential recovery as a result of ^{1}H-^{1}H NOEs combined with different relaxation rates of different protein protons (Kalk and Berendsen, 1976). This effect could be alleviated by measurement of R_1^p values only in the initial rate, i.e., by the use of short inversion-recovery delays. Measurements of R_1^p rates can further be compromised by magnetization transfer between water and amide protons, as protein-bound paramagnetic ions strongly enhance the water relaxation. This effect, which has been discussed earlier (Bertini et al., 1997; Pervushin et al., 2002; Iwahara et al., 2003), also affected the R_1^p values of the slowly relaxing amide protons in Mn^{2+}- and Gd^{3+}-EDTA-derivatized ArgN, but was hardly apparent in the Cu^{2+} complex which enhanced the water relaxation only little. In principle, it could be alleviated by recording data with selective inversion of the amide protons to ensure the same state of the water magnetization in the paramagnetic and diamagnetic samples. Considering, however, that reasonably accurate R_2^p data can be obtained for Mn^{2+}- and Gd^{3+}-complexes by simple line-width measurements of NMR cross-peaks, measurement of R_1^p data is hardly attractive for the determination of distance restraints with these metal ions.

Qualitative (Girvin and Fillingame, 1995; Papavoine et al., 1995; Ramos and Varani, 1998; Johnson et al., 1999; Battiste and Wagner, 2000; Varani et al., 2000; Liu et al. 2002) and quantitative (Bertini et al., 1996, 1997; Gillespie and Shortle, 1997b; Banci et al., 1998; Gaponenko et al., 2000; Hus et al., 2000; Donaldson et al., 2001; Iwahara et al., 2003) geometric restraints can been obtained from paramagnetic relaxation enhancements. Gillespie and Shortle (1997b) proposed the measurement of R_1^p/R_2^p ratios to obtain residue-specific effective τ_c values, followed by calculation of the metal-proton distances using Equations 2 and 3. In our hands, this approach resulted in large uncertainties of the distance values and more meaningful distance restraints were obtained by a calibration curve established in the way described by Bertini et al. (1996). This procedure converts the relaxation data into distance restraints in a way completely analogous to the conversion of NOE integrals into distance restraints by the CALIBA algorithm inside DYANA (Güntert et al., 1991). It is based on prior availability of protein structure coordinates and supported by the possbility to estimate the τ_e value accurately. The paramagnetic distance restraints derived from R_1^p values of the Cu^{2+} complex were readily accomodated by DYANA which achieved the optimization of the metal position together with the structure calculation. The Mn^{2+} data were not employed for structure refinement of ArgN. Due to their long-range nature, they present

a promising tool for the structural characterization of the ArgN-DNA complex.

The present study demonstrates that considerable structural refinements can be obtained by attachment of EDTA to a single site of the protein and measurement of R_1^p data from a single metal ion. The long-range nature of the relaxation restraints is particularly useful for the refinement of structural elements where long-range NOEs are scarce. It must be kept in mind, however, that R_1^p rates depend on interatomic distances with $1/r^6$. Just like NOEs, paramagnetic restraints thus overrepresent the shorter distances compared to the longer ones when applied to mobile regions of the protein. The problem is well known for NOEs (Bonvin et al., 1996). In the case of paramagnetic restraints, this effect is to some degree alleviated by their long-range nature, i.e., the same amplitude motion occurring far from the metal ion would affect R_1^p values less than NOEs to nearby protons (Krugh, 1979). In the case of the solvent-exposed loop of the ArgN repressor shown in Figure 3, ^{15}N-NOE measurements did not reveal any increased mobility compared to the core of the protein (data not shown), suggesting that the refined structure is more accurate. The observation of significant pseudocontact shifts with Co^{2+} (Figure 1) indicates that the linker of the chelating agent used here is relatively rigid, minimizing swaying movements of the metal ion with respect to the protein. A full evaluation of the rigidity of chelating agent and protein loop would be possible by placing the metal ion on the other side of the protein loop which could be achieved by preparation of a new protein sample with a suitably placed cysteine residue.

Acknowledgements

We thank Dr William Griffith for the analysis of derivatized ArgN by mass spectrometry and Dr Edvards Liepinsh for help with the NMR spectrometer and DYANA calculations. This work was supported by a grant from the Swedish (VR) and Australian Research Councils (ARC). G.O. acknowledges an ARC Federation Fellowship and G.P. a postdoctoral fellowship by the EU network contract HPRN-CT-2000-00092.

References

Allegrozzi, M., Bertini, I., Janik, M.B.L., Lee, Y., Liu, G. and Luchinat, C. (2000) *J. Am. Chem. Soc.*, **122**, 4154–4161.

Andersson, P., Weigelt, J. and Otting, G. (1998) *J. Biomol. NMR*, **12**, 435–441.

Banci, L., Bertini, I., Cremonini, M.A., Gori-Savellini, G., Luchinat, C., Wüthrich, K. and Güntert, P. (1998) *J. Biomol. NMR*, **12**, 553–557.

Banci, L., Bertini, I. and Luchinat, C. *Nuclear and Electronic Relaxation*, VCH, Weinheim, 1991.

Barbieri, R., Bertini, I., Cavallaio G., Lee, Y. and Luchinat, C. (2002a) *J. Am. Chem. Soc.*, **124**, 5581–5587.

Barbieri, R., Bertini, I., Lee, Y., Luchinat, C. and Velders, A.H. (2002b) *J. Biomol. NMR*, **14**, 365–368.

Battiste, J.L. and Wagner, G. (2000) *Biochemistry*, **39**, 5355–5365.

Bertini, I. and Luchinat, C. (1996) *Coord. Chem. Rev.*, **150**, 1–256.

Bertini, I., Briganti, F., Luchinat, C. and Xia, Z. (1993) *J. Magn. Reson.*, **101**, 198–201.

Bertini, I., Cavallaro, G., Cosenza, M., Kümmerle, R., Luchinat, C., Piccioli, M. and Poggi, L. (2002) *J. Biomol. NMR*, **23**, 115–125.

Bertini, I., Couture, M.M.J., Donaire, A., Eltis, L.D., Felli, I., Luchinat, C., Piccioli, I. and Rosato, A. (1996) *Eur. J. Biochem.*, **241**, 440–452.

Bertini, I., Donaire, A., Luchinat, C. and Rosato, A. (1997) *Proteins*, **29**, 348–358.

Bertini, I., Luchinat, C. and Rosato, A. (2000) *Inorg. Chim. Acta*, **297**, 199–205.

Bertrand, R., Capony, J., Derancourt, J. and Kassab, R. (1999) *Biochemistry*, **38**, 11914–11925.

Boisbouvier, J., Gans, P., Blackledge, M., Brutscher, B. and Marion, D. (1999) *J. Am. Chem. Soc.*, **121**, 7700–7701.

Bonvin, A.M. and Brunger, A.T. (1996) *J. Biomol. NMR*, **7**, 72–76.

Burgi, R., Pitera, J. and van Gunsteren, W.F. (2001) *J. Biomol. NMR*, **19**, 305–320.

Caravan, P., Ellison, J.J., McMurry, T.J. and Lauffer, R.B. (1999) *Chem. Rev.*, **99**, 2293–2352.

Donaldson, L.W., Skrynnikov, N.R., Choy, W., Muhandiram, D.R., Sarkar, B., Forman-Kay, J.D. and Kay, L.E. (2001) *J. Am. Chem. Soc.*, **123**, 9843–9847.

Dvoretsky, A., Gaponenko, V. and Rosevear, P.R. (2002) *FEBS Lett.*, **528**, 189–192.

Ebright, Y.W., Chen, Y., Ludescher, R.D. and Ebright, R.H. (1993) *Bioconj. Chem.*, **4**, 219–225.

Ebright, Y.W., Chen, Y., Pendergast, P.S. and Ebright, R.H. (1992) *Biochemistry*, **31**, 10664–10670.

Farrow, N.A., Muhandiram, R., Singer, A.U., Pascal, S.M. Kay, C.M., Gish, G., Shoelson, S.E., Pawson, T., Forman-Kay, J.D. and Kay, L.E. (1994) *Biochemistry*, **33**, 5984–6003.

Ferentz, A.E. and Wagner G. (2000) *Q. Rev. Biophys.*, **33**, 29–65.

Ferretti, J.A. and Weiss, G.H. (1989) *Meth. Enzymol.*, **176**, 3–11.

Gaponenko, V., Altieri, A.S., Li, J. and Byrd, R.A. (2002) *J. Biomol. NMR*, **24**, 143–148.

Gaponenko, V., Dvoretsky, A., Walsby, C., Hoffman, B.M. and Rosevear, P.R. (2000) *Biochemistry*, **39**, 15217–15224.

Gaponenko, V., Howarth, J., Columbus, L., Gasmi-Seabrook, G., Yuan, J., Hubbell, W.L. and Rosevear, P.R. (2000) *Protein Sci.*, **9**, 302–309.

Gaponenko, V., Sarma, S.P., Altieri, A.S., Horita, D.A., Li, J. and Byrd, R.A. (2004) *J. Biomol. NMR*, **28**, 205–212.

Gillespie, J.R. and Shortle, D. (1997a) *J. Mol. Biol.*, **268**, 158–169.

Gillespie, J.R. and Shortle, D. (1997b) *J. Mol. Biol.*, **268**, 170–184.

Girvin, M.E. and Fillingame, R.H. (1995) *Biochemistry*, **34**, 1635–1645.

Güntert, P., Braun, W. and Wüthrich, K. (1991) *J. Mol. Biol.* **217**, 517–530.

Güntert, P., Mumenthaler, C. and Wüthrich, K. (1997) *J. Mol. Biol.*, **273**, 283–298.

Hubbell, W.L. and Altenbach, C. (1994) *Curr. Opin. Struct. Biol.*, **4**, 566–573.

Hubbell, W.L., Gross, A., Langden, R. and Lietzow, M.A. (1998) *Curr. Opin. Struct. Biol.*, **8**, 649–656.

Hus, J.C., Marion, D. and Blackledge, M. (2000) *J. Mol. Biol.*, **298**, 927–936.

Ikegami, T., Verdier, L., Sakhaii, P., Grimme, S., Pescatore, B., Saxena, K., Fiebig, K.M. and Griesinger, C. (2004) *J. Biomol. NMR*, **29**, 339–349.

Iwahara, J., Anderson, D.E., Murphy, E.C. and Clore, G.M. (2003) *J. Am. Chem. Soc.*, **125**, 6634–6635.

Johnson, P.E., Brun, E., MacKenzie, L.F., Withers, S.G. and McIntosh, L.P. (1999) *J. Mol. Biol.*, **287**, 609–625.

Kalk, A. and Berendsen, H.J.C. (1976) *J. Magn. Reson.*, **24**, 343–366.

Koenig, S. H. and Brown III, R.D. (1985) *J. Magn. Reson.*, **61**, 426–431.

Krugh, T.R. (1979) In *Spin Labelling II: Theory and Applications*, Berliner, L. (Ed.), Academic Press, New York, pp. 339–372.

Liu, G., Guibao, C.D. and Zheng, J. (2002) *Mol. Cell. Biol.*, **22**, 2751–2760.

Liu, S. and Edwards, D.S. (2001) *Bioconj. Chem.*, **12**, 7–34.

Ma, C. and Opella, S.J. (2000) *J. Magn. Reson.*, **146**, 381–384.

Madhu, P.K., Grandori, R., Hohenthanner, K., Mandal, P.K. and Müller, N. (2001) *J. Biomol. NMR*, **20**, 31–37.

Mal, T.K., Ikura, M. and Kay, L.E. (2002) *J. Am. Chem. Soc.*, **124**, 14002–14003.

Martell, A.E., Smith, R.M. and Motekaitis, R.J. (1972) *NIST Critically Selected Stability Constants of Metal Complexes*, Natl. Inst. Standards and Technology.

Papavoine, C.H.M., Aelen, J.M.A., Konings, R.N.H., Hilbers, C.W. and van de Ven, F.J.M. (1995) *Eur. J. Biochem.*, **232**, 490–500.

Pervushin, K., Vögeli, B. and Eletsky A. (2002) *J. Am. Chem. Soc.*, **124**, 12898–12902.

Pintacuda, G., Hohenthanner, K., Otting, G. and Müller, N. (2003) *J. Biomol. NMR*, **27**, 115–132.

Pintacuda, G., Keniry, M.A., Huber, T., Park, A.-Y., Dixon, N.E. and Otting, G. (2004) *J. Am. Chem. Soc.*, **126**, 2963–2970.

Prosser, R.S., Bryant, H., Bryant, R.G. and Vold, R.R. (1999) *J. Magn Reson.*, **141**, 256–260.

Ramos, A. and Varani, G. (1998) *J. Am. Chem. Soc.*, **120**, 10992–10993.

Sakagami, N., Yamada, Y., Konno, T. and Okamoto, K. (1999) *Inorg. Chim. Acta*, **288**, 7–16.

Selvin, P.R. (2002) *Annu. Rev. Biophys. Biomol. Struct.*, **31**, 275–302.

Sunnerhagen, M., Nilges, M., Otting, G. and Carey, J. (1997) *Nat. Struct. Biol.*, **4**, 819–826.

Tolman, J.R., Flanagan, J.M., Kennedy, M.A. and Prestegard, J.H. (1995) *Proc. Natl. Acad. Sci.*, **92**, 9279–9283.

Varani, L., Gunderson, S.I., Mattaj, I.W., Kay, L.E., Neuhaus, D. and Varani, G. (2000) *Nat. Struct. Biol.*, **7**, 329–335.

Voss, J., Salwinski, L., Kaback, H.R. and Hubbell, W.L. (1995) *Proc. Natl. Acad. Sci.*, **92**, 12295–12299.

Wider, G., Neri, D. and Wüthrich, K. (1991) *J. Biomol. NMR*, **1**, 93–98.

Wöhnert, J., Franz, K.J., Nitz, M., Imperiali, B. and Schwalbe, H. (2003) *J. Am. Chem. Soc.*, **125**, 13338–13339.